SANDIA REPORT

SAND2002005-5356
Unlimited Release
Printed October 2005

Thin Plate Gap Bridging Study for Nd:YAG Pulsed Laser Lap Welds

Jerome T. Norris, R. Allen Roach, Phillip W. Fuerschbach, John E. Bernal

Prepared by
Sandia National Laboratories
Albuquerque, New Mexico 87185 and Livermore, California 94550

Sandia is a multiprogram laboratory operated by Sandia Corporation,
a Lockheed Martin Company, for the United States Department of Energy's
National Nuclear Security Administration under Contract DE-AC04-94AL85000.

Issued by Sandia National Laboratories, operated for the United States Department of Energy by Sandia Corporation.

Available to DOE and DOE contractors from
U.S. Department of Energy
Office of Scientific and Technical Information
P.O. Box 62
Oak Ridge, TN 37831

Telephone: (865) 576-8401
Facsimile: (865) 576-5728
E-Mail: reports@adonis.osti.gov
Online ordering: http://www.osti.gov/bridge

Available to the public from
U.S. Department of Commerce
National Technical Information Service
5285 Port Royal Rd.
Springfield, VA 22161

Telephone: (800) 553-6847
Facsimile: (703) 605-6900
E-Mail: orders@ntis.fedworld.gov
Online order: http://www.ntis.gov/help/ordermethods.asp?loc=7-4-0#online

SAND2005-5356
Unlimited Release
Printed October 2005

Thin Plate Gap Bridging Study for Nd:YAG Pulsed Laser Lap Welds

Jerome T. Norris, R. Allen Roach, Phillip W. Fuerschbach, and John E. Bernal
Materials and Process Sciences Center - Joining and Coating and
Readiness Campaign Management
Sandia National Laboratories
P.O. Box 5800
Albuquerque, New Mexico 87185-0889

Abstract

In an on going study of gap bridging for thin plate Nd:YAG laser lap welds, empirical data, high speed imaging, and computer modeling were utilized to better understand surface physics attributed to the formation and solidification of a weld pool. Experimental data indicates better gap bridging can be achieved through optimized laser parameters such as pulse length, duration, and energy. Long pulse durations at low energies generating low peak powers were found to create the highest percent of gap bridging ability. At constant peak power, gap-bridging ability was further improved by using a smaller spot diameter resulting in higher irradiances. Hence, welding in focus is preferable for bridging gaps. Gas shielding was also found to greatly impact gap-bridging ability. Gapped lap welds that could not be bridged with UHP Argon gas shielding, were easily bridged when left unshielded and exposed to only air. Incident weld angle and joint offset were also investigated for their ability to improve gap bridging. Optical filters and bright-light surface illumination enabled high-speed imaging to capture the fluid dynamics of a forming and solidifying weld pool. The effects of various laser parameters and the weld pool's interaction with the laser beam could also be observed utilizing the high-speed imaging. The work described is used to develop and validate a computer model with improved weld pool physics. Finite element models have been used to derive insight into the physics of gap bridging. The dynamics of the fluid motion within the weld pool in conjunction with the free surface physics have been the primary focus of the modeling efforts. Surface tension has been found to be a more significant factor in determining final weld pool shape than expected.

Table of Contents

List of Figures

1. Introduction

Welding of thin plate (<0.005") material is difficult regardless of joint geometry and increasingly more so for processes which provides no filler material. Given the demand for smaller and lighter manufactured components, welding of thin sheet material becomes essential however it does not lend itself to an edge or butt joint geometry: a lap joint then becomes the predominate joint design. Edge and butt joint geometries require precise part fit up in efforts to avoid gapping which leads to shine through and/or insufficient melting. In a lap joint design, gapping is only dependent upon the flatness of the contact surface, therefore lighter machining tolerances become an inherent benefit. In this study, a thin Kovar plate 0.004" thick is welded to a 0.020" thick base plate. A controlled gap of 0.002, 0.003, or 0.004" is maintained between the two plates. Since lap welds only utilize material melted from the top plate to create the joining ligament, bridging a gap 50, 75, or 100% of the top plate's thickness is not easily done.

2. Experimental Setup & Thermal Fluid Modeling

2.1 Experimental Setup: Precise fixturing and thorough laser beam characterization were required to ensure experimental accuracy. Pulse energy for each process parameter was measured prior to the experiment along with a measure of the laser beam's spot size and waist location. A Scientech Vectra S310 meter with an AC50HD detector measured the laser pulse energy. Beam spot size and waist location were determined by characterizing the beam with 0.002" Kapton film (Ref. 1). A Lasag SLS C16 pulsed Nd:YAG with a 400µm fiber delivery, real time pulse energy compensation and a 100 mm focusing lens was used. Process parameters for this study included pulse energies of 0.6 – 3.3 J, pulse lengths of 1.5 – 8.0 ms, and spot diameters of .30 – 1.0 mm; spot diameter was varied systematically by defocusing the beam, both diverging and converging. Process variables were limited to not exceeding penetration beyond the base plate's thickness and unless otherwise stated, all experiments were conducted at sharp focus with a perpendicular beam angle.

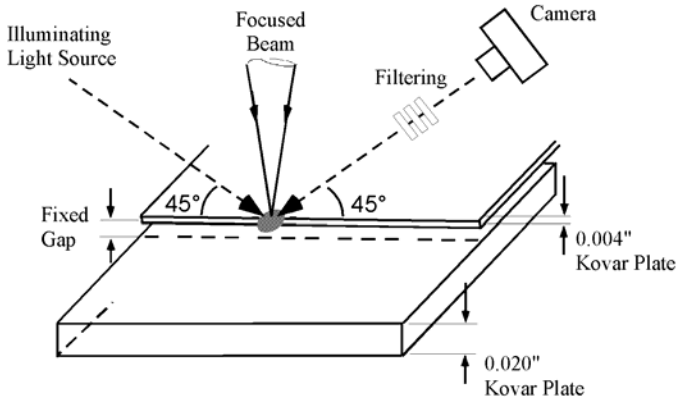

Figure 1. Schematic showing plate orientation with respect to focused beam, fiber bundle light source and high speed digital camera.

Three lap weld fixtures were used in this study with 0.002", 0.003", and 0.004" fixed gap. Each fixture was designed to hold a 0.004" top plate and a 0.020" bottom plate while maintaining the desired gap (Figure 1). To ensure flatness and sharp edges, Kovar samples were wire EDM cut,

1”X 0.5”X 0.004” and 1”X 0.5”X 0.020”, etched with a bright dip solution of acetic, nitric, and hydrofluoric acids, and stress relieved. Stress relieving of the thin plates required loading the samples (1420 g) with aluminum plates in a dry hydrogen furnace at 950°C for 60 minutes with a standard furnace cool down. Prior to welding, each sample was visually inspected under a 20X microscope. Although random testing of fixtured samples measured a flatness ±3 μm (measurements made with a Wyko laser profilometer), visual inspection insured a damaged sample was not used. Spot welds not adequately spaced reduced the fixed gap allowing sequential spots to bridge better yielding misleading gap bridging results. A 5 mm distance between each spot is necessary to negate this effect. Overall, each sample received no more then 5 weld spots.

The effect of gas shielding was evaluated. Both UHP argon and nitrogen with a flow rate of 30CFH were used along with tests run only in air – without shielding gas. Gas was delivered at approximately 45° from horizontal transverse to the joint. The effect of joint/beam alignment was investigated. These tests required that the beam be aligned off-center favoring the 0.004” top plate by approximately 25% of the beam’s diameter (Figure 2). Incident beam angle was examined perpendicular (normal) to the sample’s surface and at 15° from normal into the lap joint.

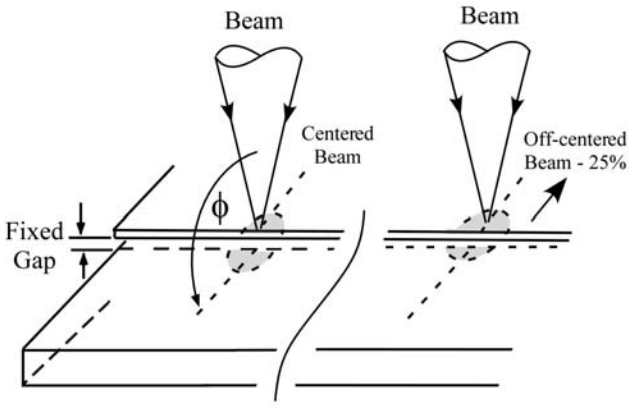

Figure 2: Schematic showing weld joint orientation to beam angle, φ, and 25% beam diameter offset.

Visualization experiments were carried out for computer model verification and to aid in the general understanding of weld pool physics. A Roper-Scientific HG-TX color CCD imager with a Navitar zoom lens was positioned in line with the weld joint at a 45° angle to the sample surface to provide imaging ~25X of that of the original spot (Figure 1). A 99% Nd:YAG reflecting mirror, #03 neutral density filter and a 540 nm notch filter were used to control the wavelength and amount of light entering into the CCD. These filters were attached at the end of the Navitar lens. A Schott-Fostec 8 mm fiber bundle light with a 150 W tungsten halogen lamp was used for surface illumination. Lighting was supplied directly opposite to that of the CCD imager as to reflect the light off the sample directly into the CCD array. Imaging capability and resolution were limited by the camera settings: 512 X 144 pixels at 2000 fps with an exposure time of 483 μs.

2.2 Thermal-Fluid Model: The finite element code (Ref. 2) modified for simulation of the laser weld process is a two- and three-dimensional finite element program which excels in analyses of multiphysical processes, particularly those involving the major branches of mechanics such as fluid/ solid mechanics, energy transport and chemical species transport. It is based on a full-Newton-coupled algorithm which allows for simultaneous solution of the governing principles, making the code ideally suited for problems involving closely coupled bulk mechanics and interfacial phenomena. For this effort, the motions of the keyhole boundaries are tracked with either an Arbitrary Lagrangian/Eulerian (ALE) formulation or the level set method for tracking moving interfaces. The level set method is well suited for the simulation of a spot or continuous weld (Ref. 3).

The boundary conditions for the momentum equation on the weld pool free surface consist of a balance of the vapor recoil force, pressure, viscous stress, and surface tension. Vapor recoil is created by the vaporization of the liquid metal after the surface of the liquid exceeds the boiling temperature of the metal. Both convective and radiative heat losses are included in the thermal boundary condition for the weld surface. The laser heat flux distribution on the material surface can be varied temporally and spatially based on the laser weld process. Latent heat release is handled by using the enthalpy method. Material properties for all materials are input as functions of temperature.

3. Results & Discussion

3.1 Measure of Gap Bridging Ability: Weld joint strength is primarily defined by the cross-sectional area of the attaching ligament between the top and bottom plates. The material making up the ligament between the two plates is drawn from the molten material created by the intersecting of the top plate and the beam. For a joint centered beam, this creates a semi-circular cut out. The semi-circle creates an arced edge in which to bridge between the two plates (Figure. 3). The ratio of joining ligament's arc length to the total arc length created by the circular beam is the "percent gap bridged". This is approximated using a Zeiss stereoscope under 30X magnification. Since percent gap bridged does not relate to changes in cross-sectional ligament areas, weld strength will also be considered when determining optimal process parameters and weld setup.

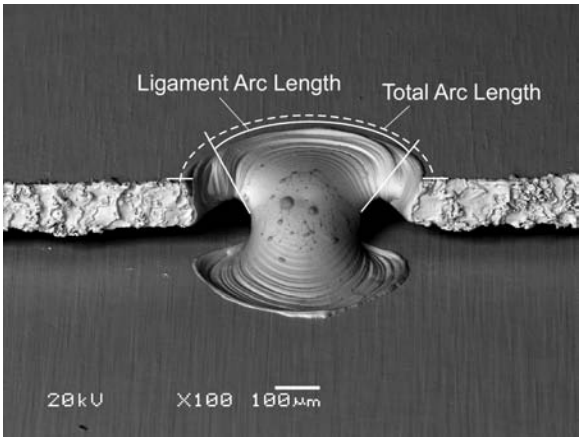

Figure 3: Successful bridged gap fillet lap weld. Ligament arc length and Total arc length are used to determine "Percent gap bridged".

3.2 Effect of Gas Shielding: Gas shielding impacted gap bridging ability the most. Argon and nitrogen shielded spot welds were unable to bridge gaps consistently over the range of parameters chosen for this study. Surface tension dominated flow resulting in a molten ball clinging to the top plate inhibited the flow of material (figure 4). For higher energy welds providing more molten material, flow to the base plate only occurred once the mass of the ball was greater than the surface tension force. This sudden flow of material would leave the bridge either unsuccessful or only slightly (<30%) attached. This is in part due to melt back phenomenon which occurs while the ball is still attached to the top plate. This is discussed further in § 3.7. Gap bridging with argon shielding was only achieved when welding at a 15° angle into the joint. § 3.6 addresses this further.

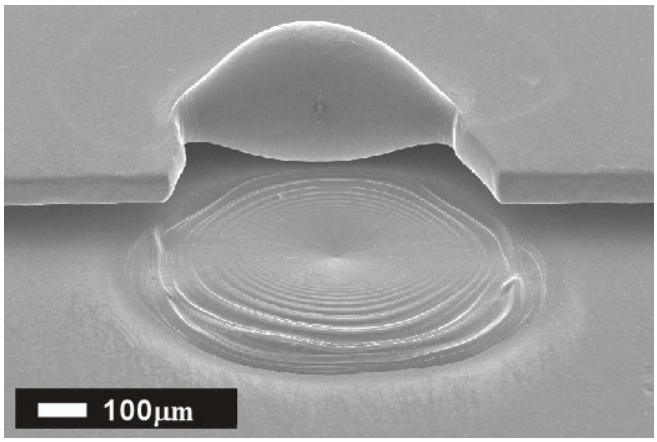

Figure 4: An unsuccessful fillet spot weld as a result of a negative surface tension gradient force resulting in melt-back of the top plate. 3.0 J, 4 ms.

Welding in air provided the best and most consistent results. A change in surface tension as a result of oxidation enabled a consistent flow of material to the base plate to form a ligament. The clinging of the molten ball to the top plate and the melt back phenomenon was not seen for welds made in air. The high repeatability for "in air" welds allowed for good correlation between bridging ability and process variables. All following results, unless otherwise stated, are responses or behaviors of welds made in air (no cover gas).

3.3 Effect of Pulse Energy and Duration: Pulse length and energy were systematically varied to determine their effect of gap bridging. Gap bridging is believed to be driven by melting rate controlled by peak power balanced against the 'dominate' weld pool force, largely influenced by shielding gas type or weld pool and beam interactions. Peak power as defined below (pulse energy (E) divided by pulse time (t_p)) was found to be a good predictor of bridging ability (Figure 5).

$$P_p = \frac{E}{t_p}$$

For a 0.004" thick top plate and a 290 μm beam diameter, percent gap bridged is optimized between 300 – 700 W peak power. Below 200 W insufficient melting inhibits bridging while above 700 W, penetration starts to approach the depth of the plate.

From the equation for peak power it can be seen that there are numerous combinations of pulse energy and time that optimize bridging. Since weld pool size is dependent upon energy absorbed (Ref. 4), longer pulse times provide more energy to form larger spot welds and yield a larger ligament. The increased cross-sectional area of the larger ligament provides greater weld joint strength. Although the percent gap bridged for long pulse times is no greater than that of a shorter time, long–pulse low–energy welds at optimized peak power's produce larger ligaments which in turn are stronger and preferable for bridging gaps.

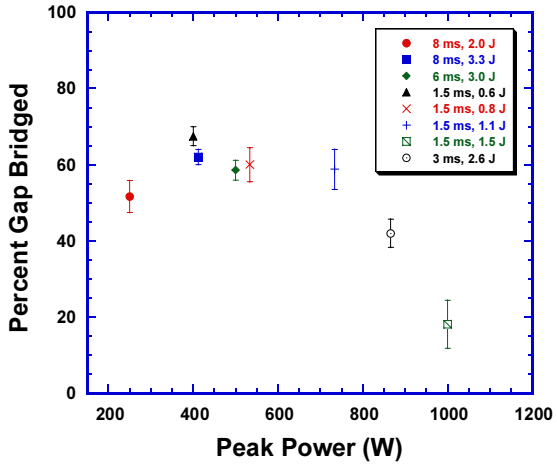

Figure 5: Effect of pulse energy and duration on gap bridging ability. 75 µm gap, sharp focus, no gas shielding.

3.4 Effect of Spot Diameter: Laser beam spot diameter was investigated for improved bridging ability by changing focus above and below the waist of a 100 mm focusing lens. Beam characterization with Kapton film allowed selection of beam diameter when welding at a known "offset" distance. A sample beam propagation profile for 525 W (2.1 J, 4.0 ms) is shown in Figure 6.

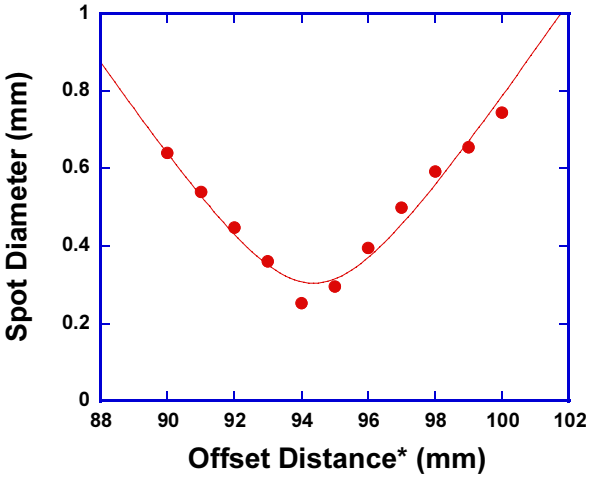

Figure 6: Kapton film (0.002" thick) Laser beam profile at 4 ms, 2.1 J. Curve fit for propagation of a multi-mode laser beam through a focusing lens (ref. 1).

At constant peak power, irradiance is maximized at sharp focus. Higher irradiance for a set peak power created better gap bridging ability. This behavior was observed under four peak power conditions (Figure 7). At a constant irradiance such as 1500 or 3000 W/mm^2, the bridging response differs for dissimilar peak powers: 500 W creates ~32% of gap bridged at 1500 W/mm^2 and only ~18% for 1000 W. High speed imaging suggests this to be due to a sudden change in weld pool physics as a result of beam and weld pool interaction disrupting the bridging ligament. Still frames from the high speed imaging are provided and explained in § 3.9.

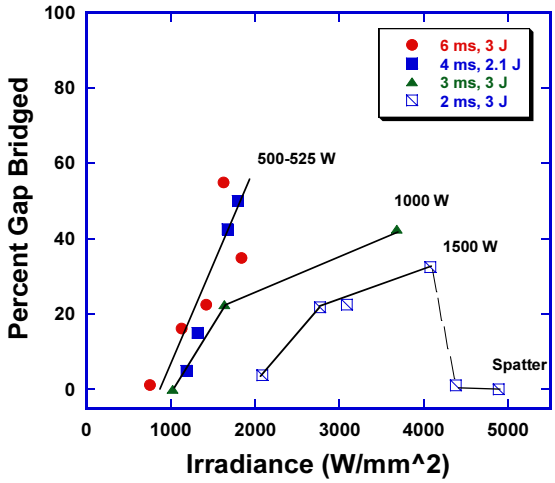

Figure 7: Effect of heat flux when holding peak power constant. 50 µm gap, varied focus, no gas shielding.

The effect of weld spatter is also shown in Figure 7. When welding at too high of an irradiance, greater than 4000 W/mm^2, molten material is thrown from the weld pool reducing the amount of material available to form a ligament making gap bridging unlikely.

3.5 Effect of Beam Location: It was observed when welding thin plate fillet lap joints that improved bridging could be achieved when welding off-center from the joint moving towards the top plate (figure 2 illustrates this further). An off-centered distance of approximately 25% of the beam's diameter was tested (Figure 8). Approximately 30 % better bridging was seen throughout the range of process variables studied. Bridging ability with respect to peak power followed a similar trend to that seen with a centered beam. Bridging cannot be achieved with peak powers below 200 W and starts dropping off after ~700 W. The improved bridging is attributed to the increased availability of filler material. By moving over ~25% of the beam's diameter, 61% more material is made available.

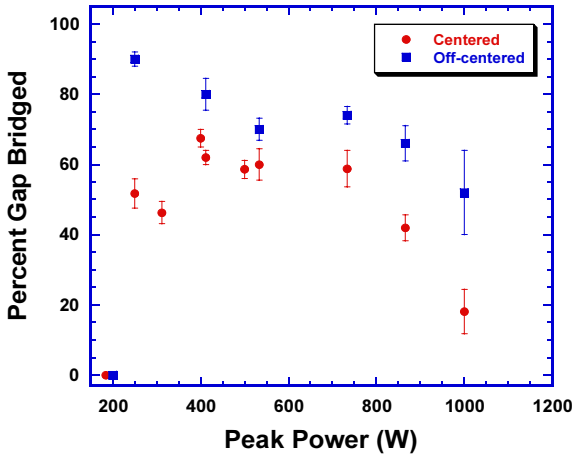

Figure 8: Welding off-center (25% of the beam's diameter to the top plate) increases gap bridging ability. 75 µm gap, sharp focus, no gas shielding.

3.6 Effect of Incident Beam Angle: The propensity for improved bridging of a 15° angled beam welding into the joint was investigated. For welds made in air, bridging ability did not follow the same trends as those of a perpendicular beam (Figure. 9). A region of high gap bridging ability over a range of peak powers was not found. A nominal 60% gap bridging was obtained at 250 W but as peak power was increased, gap bridging steadily dropped off. Variation in percent gap bridged substantially increased with the induced angle. It is expected that visualization experiments will provide more insight into this behavior.

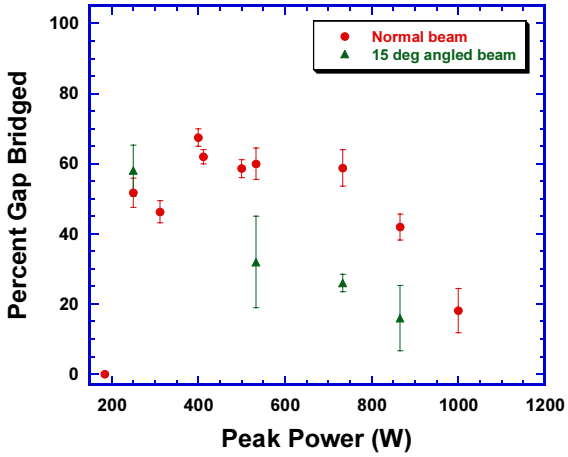

Figure 9: 15° angle reduces bridging ability and increases variability. 75 µm gap, sharp focus.

Of the process variables tested and changes made in welding conditions, an angled beam was the only condition that lead to consistent bridging with argon gas (Figure 10). Successful bridging was seen at high peak powers just prior to burn through of the base plate. Bridging was optiminzed at 850 W but quickly decreased at higher and lower peak powers. Bridging variation was still very large compared to that of "in air" perpendicular welds. It is speculated from high speed imaging that an increase in vapor pressure along with the induced beam angle drives fluid instabilities allowing for material from both the top and base plate to flow. Further visualization experiments may lend more understanding.

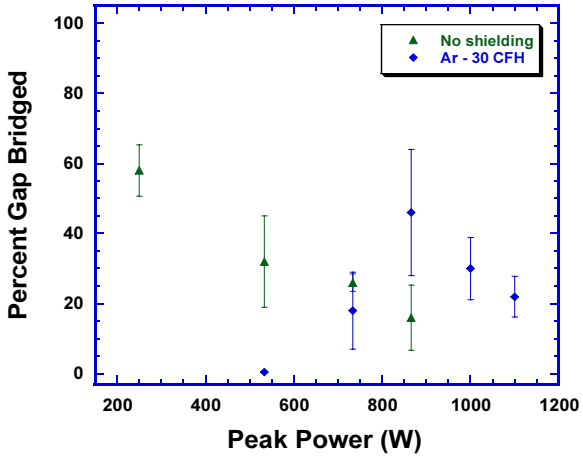

Figure 10: Effect of 15° beam angle for "in air" and argon shielded welds; 75 µm gap, Sharp focus.

3.7 Effect of Fluid Forces: Ligament formation between mating surfaces of a gapped fillet lap weld is dependent upon molten material flowing between the two plates. For this reason, fluid forces such as surface tension and vapor recoil force largely impact bridging ability. Since vapor recoil is small at low peak powers, its influence is assumed minimal for most tested parameters (Ref. 5). Surface tension however, varies upon material, temperature, and the presence of surface acting agents such as oxides (ref. 6). A negative surface tension slope with increased temperature causes a convective flow of material outward creating a molten droplet (ball) to form which clings to the top plate driving a melt back phenomenon as described in § 3.2. The molten ball inhibits the steady flow of material and as a result, the bridge is typically unsuccessful with either the ligament material remaining on the top plate or deposited entirely on the plate below. This behavior is observed for argon or nitrogen shielded welds. "In air" welds have the opposite effect. A surface tension gradient which increases with increased temperature creates an inward convective flow resulting in a weld pool which joins more quickly and is more stable. We believe a surface tension gradient driving different convective flows is what enables vastly different results. For the case of nitrogen shielded welds, although surface reactive agents are present, their influence is not sufficient to increase the surface tension with temperature gradient to a magnitude adequate for improved fluid flow.

3.8 Effect of "In Air" Welds: "In air" welds, although offering improved bridging ability, suffer from unsightly oxidation and a shift in material chemistry which may impact the mechanical properties of the weld metal. The extent to which this can occur is specific to the type of material being used and process in which it is welded. High solidification rate processes minimize these effects. A comparative hardness test between argon, nitrogen and "in air" welds on 304L showed no discernable difference in weld metal hardness. This would imply that ultimate strength of the material was unchanged. Impacts to ductility, yield strength, or its metallurgical effects to Kovar have not yet been determined.

3.9 Mechanical Effects Observed Through High Speed Imaging: Visualization experiments allow a qualitative analysis of the phenomena associated with a forming and solidifying weld pool. Higher peak power shows increased weld pool instability due to the

increased melting rate and the increasing effect of vapor recoil. Figure 11A shows a forming weld pool where the ligament material is splashed back onto the top plate as a result of these instabilities. Lower peak powers provide a smooth flow of material to the plate below maintaining a constant undisturbed ligament increasing the likeliness for bridging (Figure 11B). Images in figure 11 show the weld pool prior to the beam turning off. This is the bright spot at the center of the weld pool.

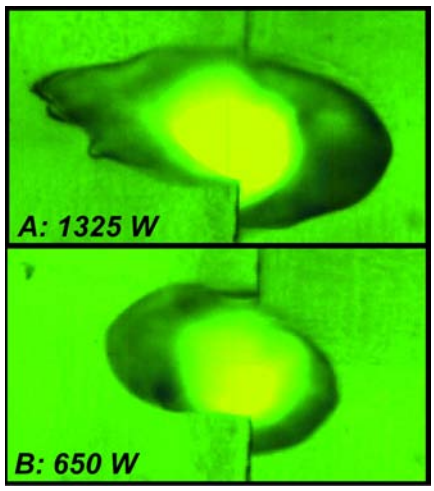

Figure 11A & B: Effect of peak power on weld pool dynamics for sharp focus welds. Camera positioned in line with the weld joint @ a 45° angle to the sample face. 50 µm gap, argon shielding, no beam angle.

Phenomena associated with the laser beam and weld pool interaction has also been observed (Figure 12). This was previously mentioned in § 3.4 concerning inconsistent bridging for similar irradiances. When the beam is larger than the weld pool (figure 12-defocused), the point at which the beam extinguishes, the weld pool is disrupted, breaking the attaching ligament or leaving it greatly reduced. Just prior to the beam being turned off, the attaching ligament is fully bridged; 0.5 ms later, the ligament is reduced to 20% of its original size. For focused welds (figure 12-focused), the beam does not appear to greatly impact the ligament. In this case, the ligament extends beyond the diameter of the beam and upon turning off, no disruption to the weld pool is evident. Changes in weld pool physics occurring for these two conditions are not currently known.

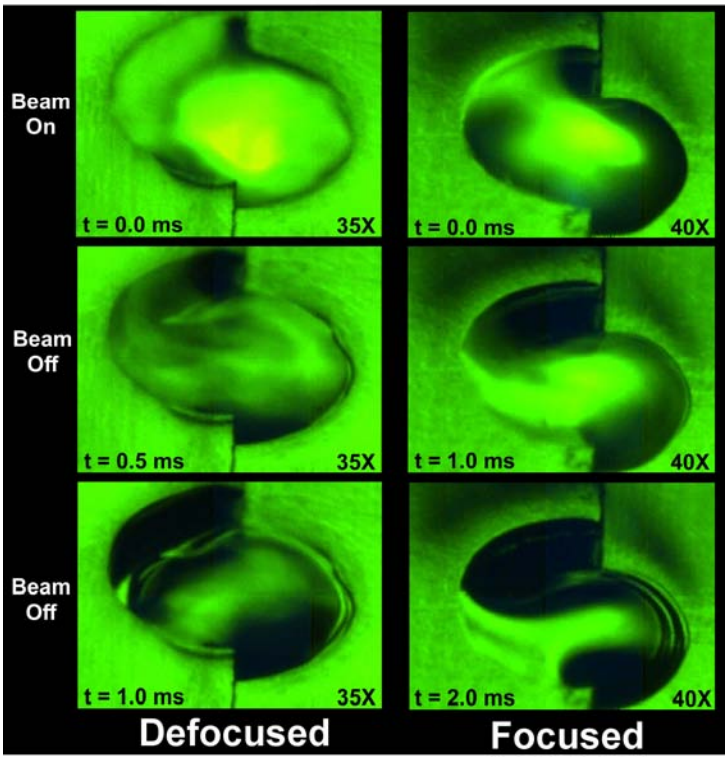

Figure 12: Weld ligament instability associated with laser beam size relative to weld pool size. 8 ms, ~825 W/mm^2.

3.10 Finite Element Modeling: Simulations were completed for both the lap joint design used in the experimental effort and a double-standing edge weld configuration. For these 2D finite element simulations, the orientation used for both geometries consisted of a slice plane normal to the face of the weld joint and through the centerline of the beam. Figure 13 shows the double-standing edge weld geometry and the mesh density used for these simulations.

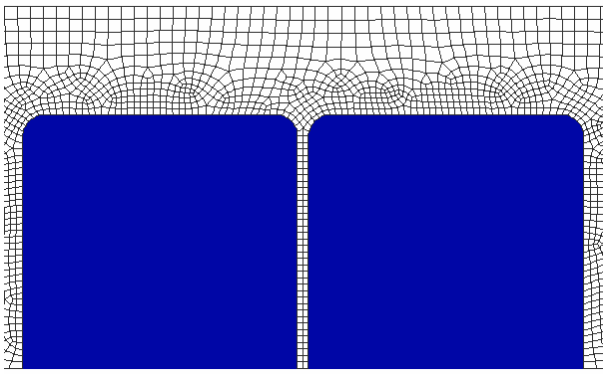

Figure 13: Double-standing edge weld geometry used in simulations to study effect of surface tension on weld pool dynamics and joining.

Results from the simulations of the lap weld joint are contained in Figure 14 and 15. Temperature scale for Figures 14 and 15 were set so molten material is shown in red and room temperature is shown in blue. The ALE formulation (§ 2.2) was utilized to track the free surface of the molten metal for the 2D lap weld simulations. As a result, the joining of the two molten pools cannot be completed due to limitations in using the ALE formulation. A successful lap weld is shown in Figure 14 for a 1000 W peak power weld with a 0.004 ms pulse using a 200 μm thick top plate. The melt-back of the top plate and the two distinct molten pools in the top and bottom plates are clearly shown in Figure 14. Joining of the plates is shown to occur at 0.0036 seconds.

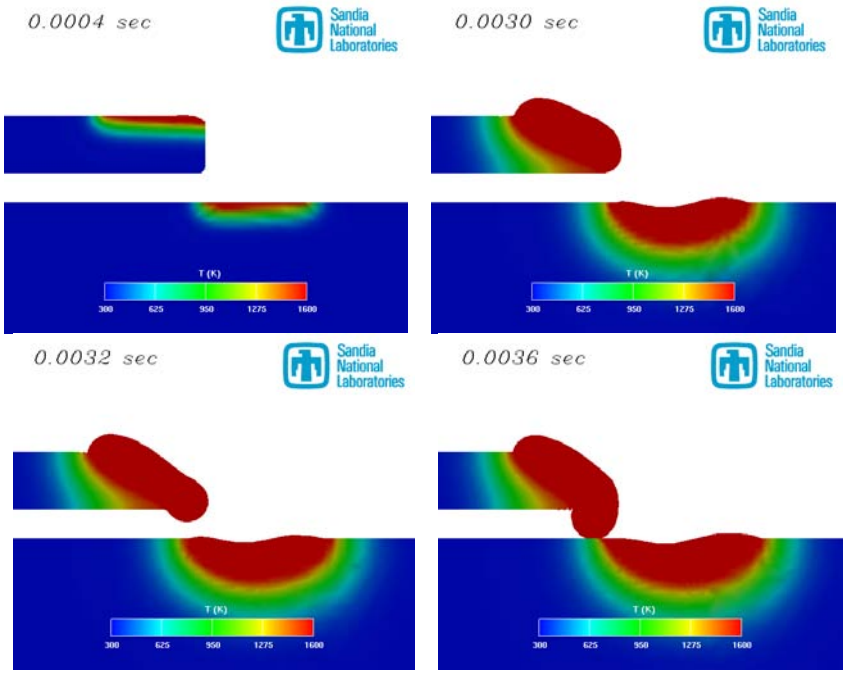

Figure 14: 2D Simulation of a successful weld using a 200 μm thick top plate. Process conditions include a 100 μm gap, laser power of 1000 W, and pulse time of 0.004 sec.

An unsuccessful lap weld is shown in Figure 15 with the same weld conditions as the successful weld but a lower peak power of 700 W. For the lower peak power weld, the melt-back of the top plate is the dominant effect. These simulations match well with the results shown in Figure 3.

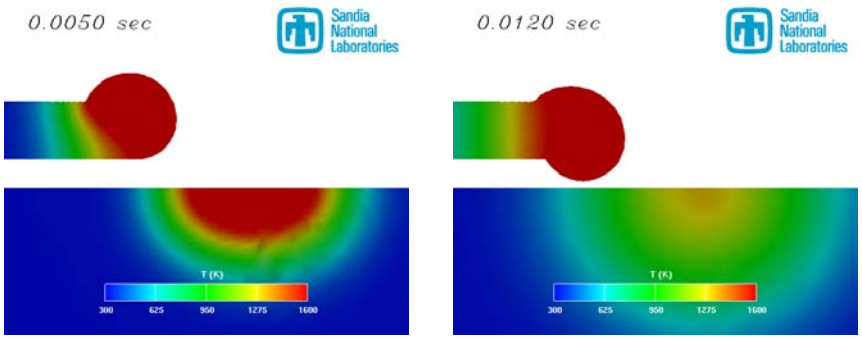

Figure 15: 2D Simulation of an unsuccessful weld using a 200 μm thick top plate. Process conditions include a 100 μm gap, laser power of 700 W, and pulse time of 0.004 sec.

Simulations of the joining process for a double-standing edge weld joint were also completed using the level set method to track the free surface of the weld pool. With the level set method the actual joining process of the two molten pools can be simulated to gain basic understanding of the dominant joining physics. Figures 16 and 17 contain simulation results of the effect of surface tension variations with temperature. Figure 16 shows simulations of a 350 W peak power weld with a 0.002 sec pulse using a constant surface tension value of 1.72 N/m. Figure 17 contains simulation results using the same peak power and pulse lengths but a variable surface tension with temperature to explore the effect of Marangoni forces on the weld pool. Comparison of the results reveal the Marangoni forces have a strong influence on the development of the molten pool. The Marangoni forces for a surface tension variation with temperature with a positive slope result in molten material being drawn to the center of the weld joint. This results in a deeper weld pool with a smaller surface diameter as shown at 0.002 sec in Figures 17. Also, the joining process occurs at an earlier time with the variable surface tension as shown by comparing the results at 0.001 sec (Figure 17). In addition, the weld pool maintains a more symmetric cross-section using a variable surface tension increasing with temperature. The cumulative effect of the deeper weld pool and increased symmetry result in a more stable pool development and a reduction in magnitude of the free surface velocities.

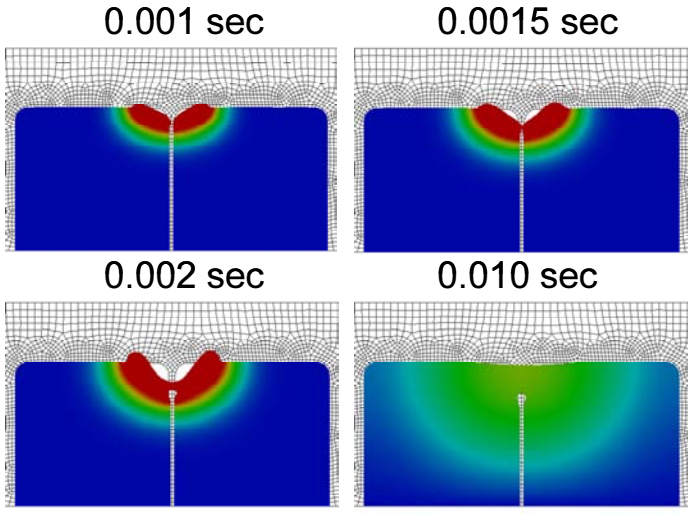

Figure 16: 2D Simulation of a double-standing edge weld using a constant surface tension value of 1.762 N/m.

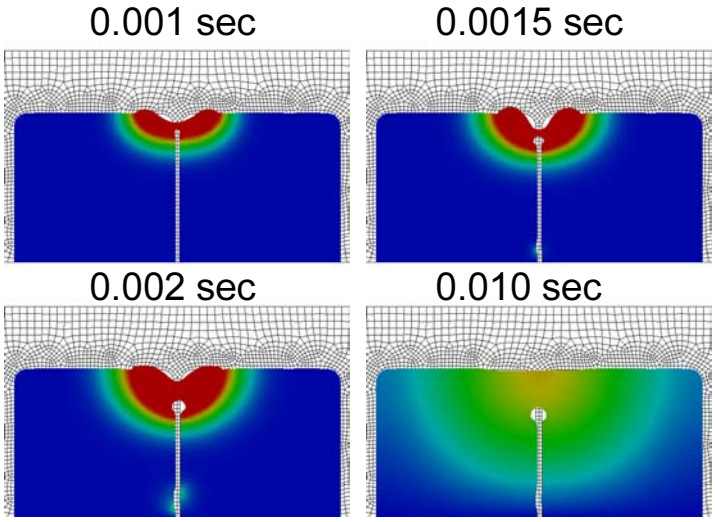

Figure 17: 2D Simulation of a double-standing edge weld using a variable surface tension with temperature of 1.762 + 0.00075*T N/m.

4. Conclusions

1) An ongoing study of gap bridging for thin plate (0.004") Nd:YAG laser lap welds has been conducted using empirical analysis, high speed imaging and computer modeling. Process variables and welding conditions studied included pulse energy (0.6 – 3.3 J); pulse duration (1.5 – 8.0 ms); welding with argon and nitrogen shielding, welding in air (no shielding); 15° incident beam angle, and welding off-center of the joint. Process variables were limited to not burning through the 0.020" base plate.
2) Varied process parameters showed gap bridging to be a function of peak power. Peak powers approximately 300 – 700 W are optimal for bridging with a 290 μm spot diameter and a 0.004" thick top plate. Longer pulse lengths provided a larger cross-sectional area to that of short pulse times resulting in a stronger weld.
3) Defocusing the beam demonstrated bridging ability was maximized when welding at sharp focus for constant peak powers.
4) Gas shielding type affected bridging ability the most. Bridging was only achieved consistently when welding in air. This is believed to be due to increased fluidity of the weld pool provided by a highly surface-reactive gas. Argon and nitrogen shielding inhibited fluid flow and were inconsistent in gap bridging.
5) Gap bridging was optimized by welding off-center from the joint favoring the top plate. Aligning off-center approximately 25% of the beam's diameter yielded a ~30% increase in bridging ability.
6) A 15° beam angle substantially reduced gap bridging potential for welds made in air. The angle increased bridging variation from one spot to the next. Argon shielded welds were able to be bridged as the result of the induce weld angle. High variation was still observed and bridging was only achieved at high peak powers just prior to burn through of the base plate.
7) Surface tension played a much larger role in gap bridging than initially expected. Computer modeling revealed improved gap bridging for highly surface reactive gases due to the increased surface tension with temperature. Argon and nitrogen shielded welds further supported the premise of surface tension effects on weld pool fluidity.

8) High speed imaging proved a valuable tool in understanding the effects of process parameters, varying welding conditions, and model validation.
9) Thermal models show burn back phenomena attributed to surface tension and its effect on fluid flow correlate well to empirical analysis and high speed imaging.

5. Acknowledgments

The authors wish to express there appreciation to Gary Pressly and Pierrette Gorman for their continued support and council through the duration of this project, David Noble and Tom Baer for their works related to the development of the FEM model and to Danny MacCallum for his careful review of this manuscript. This work was performed at Sandia National Laboratories, which is a multiprogram laboratory operated by Sandia Corporation, a Lockheed Martin Company, for the United States Department of Energy under contract DE-AC04-94AL85000.

References

1. P. W. Fuerschbach, J. T. Norris, R. C. Dykhizen, and A. R. Mahoney, *"Development and Evaluation of an In-Situ Beam Measurement for Spot Welding Lasers," Welding Journal*, Vol. 83, pp 154-159 (2004)
2. Schunk, P. R., Sackinger, P. A., Rao, R. R., Chen, K. S., Cairncross, R. A., Baer, T. A., Labreche, D. A., *GOMA 2.0- A Full-Newton Finite Element Program for Free and Moving Boundary Problems with Coupled Fluid/Solid Momentum, Energy, Mass, and Chemical Species Transport: User's Guide, Sandia Report, SAND97-2404, Sandia National Laboratories*, Albuquerque, NM, September 1998.
3. Ki, H., Mohanty, P.S., and Mazumder, J., *Metall. Mater. Trans*. A 33A, 1817-1842 (2002).
4. P. W. Fuerschbach and G. R. Eisler, *"Effects of Spot Weld Energy and Duration on Melting and Absorption," Science and Technology of Welding and Joining,* Vol. 7, pp 241-246 (2002)
5. G. A. Knorovsky, D. O. MacCallum, *"Recoil Force Measurements during Pulsed Nd:YAG Laser Spot Welds," Proceedings ICALEO,* Vol. 95, Paper I.D. 1008, (2003).
6. R. W. Messler, Jr, *Principals of Welding Processes, Physics, Chemistry, and Metallurgy*, pp 295-297, A Wiley-Interscience Publishing, Troy, NY (1999)

Distribution

3	MS 0889	J. T. Norris
1	MS 0855	R. A. Roach
1	MS 0431	P. W. Fuerschbach
1	MS 0889	J. E. Bernal
1	MS 0869	G. A. Pressly
1	MS 0869	P. H. Gorman
1	MS 0889	G. A. Knorovsky
1	MS 0889	C. V. Robino
1	MS 0889	M. Perricone
1	MS 0889	D. O. MacCallum
1	MS 0889	F. M. Hosking
2	MS 9018	Central Technical Files, 8945-1
2	MS 0899	Technical Library, 4536